frontiers | Frontiers in Energy Research

METHODS
published: 26 April 2022
doi: 10.3389/fenrg.2022.829800

Application of the Material Balance Equation Based on the BET Multimolecular Fractal Theory in a Shale Gas Reservoir

*Tingting Qiu, Shuyong Hu and Jiayi Zhang**

State Key Laboratory of Oil and Gas Reservoir Geology and Development Engineering, Southwest Petroleum University, Chengdu, China

During shale gas reservoir development, obtaining actual formation pressure is challenging; therefore, it is challenging to obtain a single well production allocation using the current formation pressure based on a productivity equation. Different shale gas reservoirs with different rock adsorption properties and the traditional Langmuir isotherm adsorption equations are not accurate in describing the adsorption properties of shale gas reservoirs, causing significant errors. BET multimolecular adsorption, considering the shale gas surface fractal dimension theory to describe the adsorption properties, can describe the adsorption surface as a multimolecular layer and regard adsorption using a fractal dimension, describing the adsorption property of shale gas more accurately. According to the core adsorption test data and theory, the actual BET multimolecular adsorption is established by considering the shale gas surface fractal dimension. Therefore, the actual material balance equation was obtained using the theory, establishing the relationship between the formation pressure and cumulative shale gas production. A time-independent distribution and cumulative gas production chart were formed using the productivity equation. Consequently, the material balance equation, which takes advantage of the BET multimolecular fractal theory, was conducted. This allocation production method obtained from the material balance equation has significant importance in shale gas development.

Keywords: Langmuir isotherm adsorption equation, BET multimolecular adsorption, fractal dimension, material balance equation, allocation production method

OPEN ACCESS

Edited by:
Lin Teng,
Fuzhou University, China

Reviewed by:
Yang Xiao,
Xi'an University of Science and Technology, China
Muhammad Wakil Shahzad,
Northumbria University, United Kingdom

****Correspondence:***
Jiayi Zhang
yixingjiatie@163.com

Specialty section:
This article was submitted to Advanced Clean Fuel Technologies, a section of the journal Frontiers in Energy Research

Received: *06 December 2021*
Accepted: *21 March 2022*
Published: *26 April 2022*

Citation:
Qiu T, Hu S and Zhang J (2022) Application of the Material Balance Equation Based on the BET Multimolecular Fractal Theory in a Shale Gas Reservoir. Front. Energy Res. 10:829800. doi: 10.3389/fenrg.2022.829800

Abbreviations: A and B, coefficient of binomial productivity equation and dimensionless parameter; B_g, natural gas volume factor, m^3/m^3; B_{gi}, original volume factor of shale gas, m^3/m^3; B_w, formation water volume factor, m^3/m^3; C, constant related to the energy of adsorption and liquefaction; C_m, shale rock compressibility factor of the matrix system; Mpa^{-1}; C_f, rock compressibility factor of the fracture system, Mpa^{-1}; C_w, formation water compressibility factor of the shale gas reservoir, Mpa^{-1}; D_s, —fractal dimension of the adsorption surface; G_f, surface free volume of the shale gas reservoir fracture system, m^3; G_m, surface free volume of the shale gas reservoir matrix system, m^3; M, —salinity of formation water, mg/L; n, adsorption layer of the gas surface; N_1, adsorption capacity of layer One; N_i, adsorption capacity of layer i; p_0, saturated vapor pressure, MPa; P_{cd}, critical desorption pressure, MPa; P_i, original formation pressure, MPa; P_S, pressure, $MPa \times 10$; R_s, natural gas solubility in the formation water, m3/m3Rsi, original formation water solubility of the shale gas reservoir, m^3/m^3; S_{wf}, water saturation of the shale gas reservoir fracture system, %; T, temperature, $^{\circ}$C; V_S, single well control volume of the shale rock, m^3; x, relative pressure $\frac{p}{p_0}$, MPa/MPa; ρ_s, density of shale, g/cm^3.

INTRODUCTION

Shale gas reserves comprised free, adsorbed, and dissolved gases, of which free and adsorbed gases are the main parts (Taghavinejad et al., 2020); (Mengal and Wattenbarger, 2011); (Huang and Zhao, 2017); (Boadu, 2000); (Sanyal et al., 2006); (Curtis, 2002); (Jenkins and Boyer, 2008). In this regard, the study of shale gas adsorption behavior is significant to reservoir volume calculation and development (Huang and Zhao, 2017); (Shao et al., 2017); (Wu et al., 2015). Currently, the Langmuir isotherm, BET equations, and other modified Langmuir and BET equations predominantly describe the adsorption behavior (Li et al., 2020); (Jaroniec et al., 1989); (Zhang et al., 2015). The classic Langmuir equation assumes that methane is monolayer-adsorbed, and the surface of the adsorbent is homogeneous with constant adsorption heat (Langmuir, 1918); (Langmuir, 2015). The adsorption behavior of shale gas is complex, and Langmuir's isotherm adsorption equation is too ideal and cannot describe it accurately. The BET adsorption theory considers the adsorption surface as a multilayer, and the adsorption capacity of every layer is the same (Myers, 1968); (Brunauer et al., 1940); (Zhou et al., 2019); (Myers and Prausnitz, 1965); (Ritter and Yang, 1987); (Dang et al., 2020). To simulate the enrichment and production of methane in shale gas reservoirs, an accurate gas adsorption model is critically required (Chareonsuppanimit et al., 2012), (Clarkson and Haghshenas, 2013), (Huang et al., 2018a). Fortunately, the BET multi-molecular fractal theory, considering the surface fractal dimension of shale gas, can describe adsorption more accurately by considering the multilayer and fractal dimension of shale gas adsorption (Brunauer et al., 1938), (Wang et al., 2022), (Chai et al., 2019), (Zheng et al., 2019), (Wang et al., 2016), (Fan and Liu, 2021). Therefore, the material balance equation can enhance the accuracy of future reservoir prediction about reserves and formation pressure based on the adsorption theory (Zhang et al., 2017), (Canel and Rosbaco, 2006), (Fianu et al., 2019).

Ambrose et al., (2012), (Xiong et al., 2021), and (Memon et al., 2020) combined the Langmuir adsorption isotherm with the volume for free gas and formulated a new gas-in-place equation accounting for the pore space occupied by the adsorbed phase; however, the adsorption surface layer and fractal dimension were not considered (Pang et al., 2019). The material balance equation proposed by Daniel et al. (Orozco and Aguilera, 2015) simultaneously considered stress-dependent porosity and permeability, free gas, adsorbed gas, and dissolved gas but also excluded the adsorption surface layer and fractal dimension. Usually, the material balance equation combined with the shale gas productivity equation is used to calculate the reservoir reserves and conduct the relevant model for predicting the production rate and formation pressure versus time (Sun et al., 2019), (Gu et al., 2014), (Hu et al., 2019). The shale gas well allocation is usually based on this method to carry out well productivity tests (Deng et al., 2014), (Wheaton, 2019). According to the test, the shale gas well binomial productivity formula is determined. If the present reservoir pressure is calculated by the material balance equation, then the actual open flow capacity of a single well can be calculated. The reasonable gas well allocation is also determined. Nevertheless,

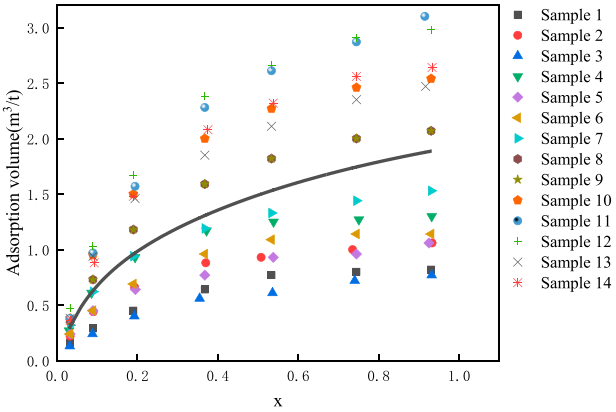

FIGURE 1 | Actual isotherm adsorption curve of shale gas Block XX.

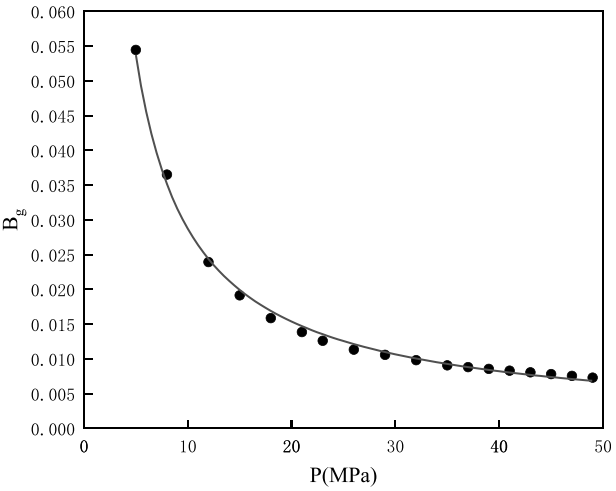

FIGURE 2 | Curve of the gas volume factor versus formation pressure of shale gas Block XX.

practical reservoir production requires convenient and efficient allocation progress. The aforementioned method aims at a certain moment, is complex, and cannot satisfy the practical production needs. Therefore, finding an efficient and convenient shale gas allocation method for the whole well life is necessary.

Huang et al. (2018b) proposed a new method. Shale reservoirs were depicted by the De Swaan dual porosity model, where the secondary and hydraulic fractures were characterized by discrete units to conduct the shale gas well productivity equation. This method can calculate more efficiently than the Eclipse simulator. Furthermore, it can describe the complex fracture network more correctly even though the calculating process and single shale gas well allocation of every production moment are complex. Sang et al. (2014) used a numerical model considering desorption and adsorption processes to establish and solve, under polar coordinates and Laplace space, respectively, predicting the

TABLE 1 | Test data of shale gas Block XX.

Sample	Pressure (MPa)	Adsorption volume (m^3/t)	Sample	Pressure (MPa)	Adsorption volume (m^3/t)
Sample 1	0.38	0.16	Sample 8	0.38	0.36
	1.04	0.29		1.04	0.73
	2.21	0.45		2.21	1.18
	4.28	0.64		4.28	1.59
	6.21	0.77		6.21	1.82
	8.67	0.8		8.67	2
	10.83	0.82		10.83	2.07
Sample 2	0.38	0.22	Sample 9	0.38	0.36
	1.05	0.44		1.04	0.73
	2.25	0.66		2.21	1.18
	4.31	0.88		4.28	1.59
	5.91	0.93		6.21	1.82
	8.56	1		8.67	2
	10.86	1.06		10.83	2.07
Sample 3	0.37	0.13	Sample 10	0.38	0.38
	1.03	0.24		1.04	0.95
	2.24	0.4		2.21	1.5
	4.13	0.56		4.28	2
	6.24	0.61		6.21	2.27
	8.62	0.72		8.67	2.46
	10.85	0.77		10.83	2.54
Sample 4	0.35	0.27	Sample 11	0.38	0.47
	1	0.61		1.04	1.03
	2.26	0.93		2.21	1.67
	4.33	1.17		4.28	2.38
	6.27	1.25		6.21	2.66
	8.74	1.27		8.67	2.91
	10.85	1.3		10.83	2.98
Sample 5	0.38	0.24	Sample 12	0.38	0.47
	1.04	0.45		1.04	1.03
	2.27	0.64		2.21	1.67
	4.28	0.77		4.28	2.38
	6.26	0.93		6.21	2.66
	8.67	0.96		8.67	2.91
	10.77	1.06		10.83	2.98
Sample 6	0.38	0.24	Sample 13	0.38	0.38
	1.04	0.45		1.04	0.94
	2.21	0.69		2.26	1.46
	4.28	0.96		4.28	1.85
	6.21	1.09		6.21	2.11
	8.67	1.14		8.67	2.35
	10.83	1.14		10.67	2.47
Sample 7	0.38	0.32	Sample 14	0.38	0.36
	1.04	0.62		1.08	0.88
	2.21	0.94		2.21	1.48
	4.28	1.19		4.37	2.08
	6.21	1.33		6.26	2.32
	8.67	1.44		8.67	2.56
	10.83	1.53		10.86	2.64

productivity of volume-fractured horizontal wells in shale gas reservoirs. This model can predict the production rate versus time, but the allocation production of the single well cannot be obtained. At present, the existing allocation methods combining the material balance equation with productivity formula cannot offer well the allocation of well life and satisfy the convenience of practical allocation apart from numeric simulation, decline analysis, and so on (Huang et al., 2018b); (Arps, 1945). As for the adsorption of shale gas reservoirs, we adopted the BET multi-molecular fractal theory. Creatively, we developed a material balance equation based on the BET multi-molecular fractal theory, considering the dissolved gas of the formation water. Furthermore, we combined this new material balance equation with the productivity equation to obtain single well allocation production versus cumulative gas production for the well life cycle. As a result, we can offer the shale gas development worker an allocation plate, and there is no need for paying attention to complex equations about the well and gas reservoir properties. In a word, this method can not only calculate the adsorption gas volume but also propose

TABLE 2 | Formation physics and fluid property of Well #1 shale gas Block XX.

Parameter	Symbol	Unit	Value	Parameter classification
Surface-free volume of the shale gas reservoir matrix system	G_m	m^3	$G_m + G_f = 1.97 \times 10^7$	Shale gas geological parameter
Surface-free volume of the shale gas reservoir fracture system	G_f	m^3		
Original volume factor of shale gas	B_{gi}	m^3/m^3	0.0069	
Formation water compressibility factor of the shale gas reservoir	C_w	Mpa^{-1}	0.000453	
Shale rock compressibility factor of the matrix system	C_m	Mpa^{-1}	0.000419	
Original formation water solubility of the shale gas reservoir	R_{si}	m^3/m^3	0.647887	
Original formation pressure	P_i	*MPa*	48.6	
Water saturation of the shale gas reservoir fracture system	S_{wf}	%	45	
Rock compressibility factor of the fracture system	C_f	Mpa^{-1}	0.000419	
Formation water volume factor	B_w	m^3/m^3	0.993262	
Density of shale	ρ_s	g/cm^3	2.65	
Critical desorption pressure	P_{cd}	*MPa*	12.58	
Single well control volume of the shale rock	V_S	m^3	$4{,}382 \times 10^4$	
Natural gas volume factor	B_g	m^3/m^3	Variable	Shale gas geological parameter
Present solubility of formation water	R_s	m^3/m^3	Variable	
Coefficient of the binomial productivity equation	A	Dimensionless parameter	1.8633×10^{-8}	Test parameter
Coefficient of the binomial productivity equation	B	Dimensionless parameter	5.78×10^{-3}	

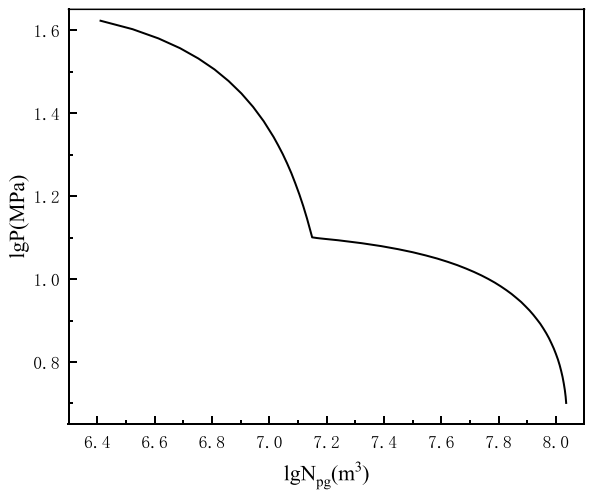

FIGURE 3 | Formation pressure versus the cumulative gas production double logarithm chart of Well #1 shale gas Block XX.

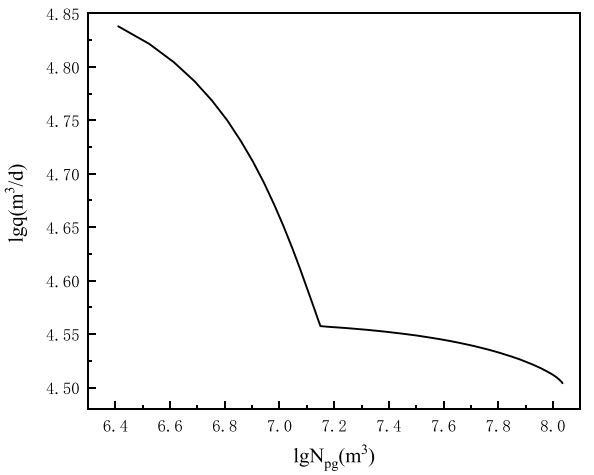

FIGURE 4 | Allocation production versus the cumulative gas production double logarithm chart of Well #1 shale gas Block XX.

a convenient and fast life cycle allocation method for shale gas reservoirs.

MATERIAL BALANCE EQUATION OF A SHALE GAS WELL BASED ON THE BET MULTI-MOLECULAR FRACTAL THEORY

The material balance equation of the confining shale gas reservoir was established by considering the reservoir as a fracture-matrix dual system and the dissolved gas in the formation water to obtain the chart of shale gas dynamic allocation production. Furthermore, the BET multimolecular and fractal adsorption theory described the gas adsorption behavior.

The Actual Isotherm Adsorption Curve of Shale Gas Block XX

Brunauer et al. (1940) proposed the BET multimolecular adsorption theory in 1940, and it was an addition to the Langmuir monolayer molecular adsorption equation. The assumption of the BET multimolecular adsorption theory is as follows:

1) The gas adsorption is multimolecular, and it does not have to cover the first layer completely and then the second.
2) The heat of adsorption (E_1) of the first layer is a certain value; the other is the liquefaction heat (E_L) of the adsorbate.
3) The adsorption and desorption of the adsorbate are exposed on the surface of the gas phase directly.

Consequently, the BET multimolecular adsorption expression is described in **Eq. 1**.

$$\frac{V}{V_m} = \frac{Cx[1-(n+1)x^n + nx^{n+1}}{(1-x)[1+(C-x)-Cx^{n+1}]}. \quad (1)$$

In the equation, x is the relative pressure $\frac{p}{p_0}$, p_0 is the saturated vapor pressure, n is the adsorption layer of the gas surface, and C is the constant related to the energy of adsorption and liquefaction.

Eq. 2 shows the relationship of the adsorption capacity between layers i and One proposed by Fripiat et al., (1986) and (Zhou et al., 2019) based on numeric simulation.

$$f_i = \frac{N_i}{N_1} = i^{-(D_s-2)}. \quad (2)$$

In **Eq. 2**, D_s is the fractal dimension of the adsorption surface, N_1 is the adsorption capacity of layer One, and N_i is the adsorption capacity of layer i. Therefore, the BET multimolecular adsorption, considering the fractal dimension of the adsorption surface expression, was obtained as **Eq. 3**.

$$V = \frac{V_m C \sum_{i=1}^{n} i^{2-D_s} \sum_{j=i}^{n} x^j}{1 + C\sum_{i=1}^{n} x^i}. \quad (3)$$

According to **Eq. 3**, the actual isotherm adsorption curve of shale gas Block XX can be obtained by regression, as shown in **Eq. 4**, and **Figure 1** shows the curve. The gas adsorption test data is showed in **Table 1**. According to the regression results, we obtained the following conclusions. The adsorption volume of shale gas Block XX was 1.19924 m^3/t, and the constant related to the energy of adsorption and liquefaction was 9.86193, based on the fractal dimension 2.5 and the layer of surface molecular adsorption 3 (**Figure 1**).

$$V = 1.19924\frac{9.86193 \times \left[\frac{P}{P_0} + \left(\frac{P}{P_0}\right)^2 + \left(\frac{P}{P_0}\right)^3 + 2^{2-2.5}\left(\left(\frac{P}{P_0}\right)^2 + \left(\frac{P}{P_0}\right)^3\right) + 3^{2-2.5}\left(\frac{P}{P_0}\right)^3\right]}{1 + 9.86193 \times \left[\left(\frac{P}{P_0}\right) + \left(\frac{P}{P_0}\right)^2 + \left(\frac{P}{P_0}\right)\right]}. \quad (4)$$

Material Balance Equation of Shale Gas Block XX

The assumption of the material balance equation of shale gas Block XX is as follows:

1) The shale gas reservoir is an isotherm system; in other words, the reservoir temperature is unchanged during exploitation.
2) The water saturation of the matrix and fracture system is different.
3) There is no formation of water to be produced.

According to the principle of the material balance equation, the underground volume of the produced shale gas comprised underground expansion, including free gas, formation water, rock, dissolved gas of formation water underground volume variation of the matrix, and fracture system. For the shale gas reservoir, it included the underground adsorption gas volume variation of the matrix system. When the shale gas reservoir proceeded to desorption, the material balance equation was as shown in **Eq. 5**.

$$\begin{aligned}
&G_{pg}B_g = G_m\left(B_g - B_{gi}\right) + G_m B_{gi}\frac{C_w S_{mwi}}{1-S_{mwi}}(P_i - P) + \\
&G_m B_{gi}\frac{C_m}{1-S_{mwi}}(P_i - P) + \frac{G_m B_{gi}}{(1-S_{mwi})B_w}S_{mwi}(R_{si} - R_s)B_g + \\
&G_f\left(B_g - B_{gi}\right) + G_f B_{gi}\frac{C_w S_{fwi}}{1-S_{fwi}}(P_i - P) + \\
&G_f B_{gi}\frac{C_f}{1-S_{fwi}}(P_i - P) + \frac{G_f B_{gi}}{\left(1-S_{fwi}\right)B_w}S_{fwi}(R_{si} - R_s)B_g \\
&+\rho_s V_S\left\{V_m\frac{C\left[\frac{P_{cd}}{P_0} + \left(\frac{P_{cd}}{P_0}\right)^2 + \left(\frac{P_{cd}}{P_0}\right)^3 + 2^{2-D_s}\left(\left(\frac{P_{cd}}{P_0}\right)^2 + \left(\frac{P_{cd}}{P_0}\right)^3\right) + 3^{2-D_s}\left(\frac{P_{cd}}{P_0}\right)^3\right]}{1 + C\left[\frac{P}{P_0} + \left(\frac{P}{P_0}\right)^2 + \left(\frac{P}{P_0}\right)^3\right]}\right. \\
&\left. - \frac{C\left[\frac{P}{P_0} + \left(\frac{P}{P_0}\right)^2 + \left(\frac{P}{P_0}\right)^3 + 2^{2-D_s}\left(\left(\frac{P}{P_0}\right)^2 + \left(\frac{P}{P_0}\right)^3\right) + 3^{2-D_s}\left(\frac{P}{P_0}\right)^3\right]}{1 + C\left[\frac{P}{P_0} + \left(\frac{P}{P_0}\right)^2 + \left(\frac{P}{P_0}\right)^3\right]}\right\}.
\end{aligned} \quad (5)$$

The high-pressure fluid parameter testing of shale gas Block XX regressed the relationship between the gas volume factor and formation pressure. **Eq. 6** shows the function, and **Figure 2** shows the curve of the gas volume factor versus the formation pressure.

$$B_g = 0.22919P^{-0.902}. \quad (6)$$

The empirical formula of the formation water property is as suggested by Yuanqian (Chen, 1990) and (Myers and Prausnitz, 1965), as shown in **Eq. 7**.

$$\begin{aligned}
R_s = (T, M, P) &= -3.1670 \times 10^{-10}T^2 \times M + 1.997 \times 10^{-8}T \times M \\
&+1.0635 \times 10^{-10}P_S^2 \times M - 9.7764 \times 10^{-8}P_S \times M + 2.9745 \times 10^{-10}T \times P_S \times M \\
&+1.6230 \times 10^{-4}T^2 - 2.7879 \times 10^{-2}T - 2.0587 \times 10^{-5}P_S^2 \\
&+1.7323 \times 10^{-2}P_S + 9.5233 \times 10^{-6}T \times P_S + 1.1937.
\end{aligned} \quad (7)$$

In the equation, R_s is the natural gas solubility in the formation water (m^3/m^3). T is the temperature (°C). P_S is the pressure ($MPa \times 10$), and M is the salinity of formation water (mg/L).

PRACTICAL MATERIAL BALANCE EQUATION OF SHALE GAS BLOCK XX

Based on the BET multimolecular adsorption theory equation (**Eq. 4**) of shale gas Block XX, the practical material balance equation of the shale gas Block XX can be established by considering the dissolved gas of formation water and adsorption of shale gas. The practical material balance

TABLE 3 | Cumulative gas production versus the formation pressure and single well allocation production.

Cumulative gas production (m^3)	Formation pressure (MPa)	Allocation (m^3/d)
2,560,459	42	68,913
3,336,274	40	66,310
4,112,330	38	63,735
4,888,812	36	61,191
5,665,926	34	58,684
6,443,905	32	56,218
7,223,014	30	53,799
8,003,557	28	51,432
8,785,884	26	49,127
9,570,407	24	46,891
10,357,608	22	44,735
10,752,390	21	43,691
11,148,069	20	42,672
11,544,735	19	41,680
11,942,493	18	40,716
12,341,457	17	39,782
12,741,758	16	38,882
13,143,541	15	38,016
13,546,976	14	37,189
13,952,255	13	36,401
14,116,546	12.6	36,098
14,676,689	12.55	36,060
15,045,356	12.53	36,045
15,596,469	12.5	36,023
17,421,447	12.4	35,949
21,040,933	12.2	35,802
24,626,119	12	35,656
28,175,327	11.8	35,513
31,686,804	11.6	35,371
35,158,721	11.4	35,231
38,589,165	11.2	35,093
41,976,138	11	34,957
45,317,553	10.8	34,823
48,611,233	10.6	34,691
51,854,902	10.4	34,560
55,046,184	10.2	34,432
58,182,599	10	34,306
61,261,559	9.8	34,182
64,280,362	9.6	34,060
67,236,190	9.4	33,940
70,120,077	9.2	33,822
72,940,198	9	33,706
75,688,122	8.8	33,593
78,360,507	8.6	33,481
80,953,874	8.4	33,372
83,464,591	8.2	33,265
85,888,877	8	33,161
88,222,791	7.8	33,058
90,462,228	7.6	32,958
92,602,913	7.4	32,860
94,640,393	7.2	32,765
96,570,033	7	32,671
98,387,010	6.8	32,581
100,086,302	6.6	32,492
101,662,682	6.4	32,406
103,110,711	6.2	32,323
104,424,729	6	32,242
105,598,839	5.8	32,163
106,626,904	5.6	32,087
107,502,526	5.4	32,013
108,219,034	5.2	31,942
108,769,462	5	31,873

equation of Well #1 Block XX was obtained from **Eq. 8** by substituting **Eqs 6** and **7** into **Eq. 5**.

$$
\begin{aligned}
&G_{pg}\times 0.22919P^{-0.902}=G_m\left(0.22919P^{-0.902}-B_{gi}\right)+\\
&G_mB_{gi}\frac{C_wS_{mwi}}{1-S_{mwi}}\left(P_i-P\right)+G_mB_{gi}\frac{C_m}{1-S_{mwi}}\left(P_i-P\right)+\\
&\frac{G_mB_{gi}}{(1-S_{mwi})B_w}S_{mwi}\left(R_{si}-\begin{pmatrix}3.1670\times10^{-10}T^2\times M+1.997\times10^{-8}T\times M+\\1.0635\times10^{-10}P_S^2\times M-9.7764\times10^{-8}P_S\times M+\\2.9745\times10^{-10}T\times P_S\times M+1.6230\times10^{-4}T^2-\\2.7879\times10^{-2}T-2.0587\times10^{-5}P_S^2+\\1.7323\times10^{-2}P_S+9.5233\times10^{-6}T\times P_S+1.1937\end{pmatrix}\right)\\
&0.22919P^{-0.902}+G_f\left(0.22919P^{-0.902}-B_{gi}\right)+G_fB_{gi}\frac{C_wS_{fwi}}{1-S_{fwi}}\left(P_i-P\right)+\\
&G_fB_{gi}\frac{C_f}{1-S_{fwi}}\left(P_i-P\right)+\frac{G_fB_{gi}}{\left(1-S_{fwi}\right)B_w}S_{fwi}\\
&\left(R_{si}-\begin{pmatrix}3.1670\times10^{-10}T^2\times M+1.997\times10^{-8}T\times M+\\1.0635\times10^{-10}P_S^2\times M-9.7764\times10^{-8}P_S\times M+\\2.9745\times10^{-10}T\times P_S\times M+1.6230\times10^{-4}T^2-\\2.7879\times10^{-2}T-2.0587\times10^{-5}P_S^2+\\1.7323\times10^{-2}P_S+9.5233\times10^{-6}T\times P_S+1.1937\end{pmatrix}\right)\times\\
&0.22919P^{-0.902}+\rho_sV_S\left\{\frac{V_m}{1+C\left[\frac{P_{cd}}{P_0}+\left(\frac{P_{cd}}{P_0}\right)^2+\left(\frac{P_{cd}}{P_0}\right)^3\right]}\begin{bmatrix}C\begin{bmatrix}\frac{P_{cd}}{P_0}+\left(\frac{P_{cd}}{P_0}\right)^2+\left(\frac{P_{cd}}{P_0}\right)^3+\\2^{2-D_s}\left(\left(\frac{P_{cd}}{P_0}\right)^2+\left(\frac{P_{cd}}{P_0}\right)^3\right)+\\3^{2-D_s}\left(\frac{P_{cd}}{P_0}\right)^3\end{bmatrix}\end{bmatrix}\right.\\
&\left.-\frac{1}{1+C\left[\frac{P}{P_0}+\left(\frac{P}{P_0}\right)^2+\left(\frac{P}{P_0}\right)^3\right]}\begin{bmatrix}C\begin{bmatrix}\frac{P}{P_0}+\left(\frac{P}{P_0}\right)^2+\left(\frac{P}{P_0}\right)^3+\\2^{2-D_s}\left(\left(\frac{P}{P_0}\right)^2+\left(\frac{P}{P_0}\right)^3\right)+\\3^{2-D_s}\left(\frac{P}{P_0}\right)^3\end{bmatrix}\end{bmatrix}\right\}.
\end{aligned}
\tag{8}
$$

According to the formation of physics and fluid properties (**Table 2**), the practical material balance equation can be established, and a double logarithm chart (allocation versus cumulative gas production) can be obtained. Therefore, the allocation of a single shale gas well can be calculated according to the cumulative gas production using the chart in the progress of shale gas exploitation.

From the productivity test data, the gas well productivity equation was as in **Eq. 9**.

$$P^2-P_{wf}^2=Aq^2+Bq. \tag{9}$$

The 1/5 times of the gas well open flow was often used as the allocation *in situ* production; therefore, the production allocation formula was as in **Eq. 10**.

$$q=\frac{1}{5}\cdot\left(\frac{-B+\sqrt{B^2+4A\left(P^2-0.1^2\right)}}{2A}\right). \tag{10}$$

CASE STUDY

As the description of the practical material balance equation of shale gas Block XX, at first, the shale gas material balance equation is conducted, considering multimolecular fractal adsorption about the single shale gas well. Second, the binomial productivity equation is obtained by regressing the productivity test data. Third, cumulative gas productivity is substituted into the first step regarding the material balance equation in order to obtain the present reservoir pressure. Fourth, the pressure is substituted into the second step productivity equation, and the single well allocation can be calculated. Finally, the abovementioned steps are repeated, and then, the allocation plate allocation production versus cumulative gas production double logarithm is drawn. According to the plate, the practical allocation process is guided quickly. The specific procedures are as follows.

Figures 3, **4** and **Table 3** show the cumulative gas production chart versus formation pressure and single well production allocation chart taking advantage of **Eqs 8–10**.

By viewing the cumulative gas production in **Figure 4**, the allocation production can be obtained. Through analysis, in **Figure 3**, the decrease in the formation pressure on the cumulative gas production was gentle, and the allocation on cumulative gas production decreased similar to that in **Figure 4** when the shale gas reservoir entered desorption. Thus, the formation pressure can keep well after desorption, and shale gas had a long dependable crop time.

CONCLUSION

Based on the practical BET multimolecular adsorption, considering the fractal dimension of the adsorption surface, a production allocation chart about Well #1 shale gas Block XX can be established using the material balance equation. The conclusions are as follows:

1) The adsorption volume of the shale gas Block XX was 1.19924 m^3/t, and the constant related to the energy of adsorption and liquefaction was 9.86193, based on the fractal dimension 2.5 and the layer of surface molecular adsorption 3.
2) According to the production allocation chart of Well #1 shale gas Block XX, before the shale gas reservoir entered the desorption, the desorption pressure decreased faster, and the cumulative gas production increased slowly. However, when the reservoir entered the desorption stage, the decrease in the formation pressure was gentle, despite the low formation pressure. Furthermore, the shale gas production allocation can maintain a certain time, indicating that most

shale gas of the production well was exploited during the desorption stage.

DATA AVAILABILITY STATEMENT

The original contributions presented in the study are included in the article/Supplementary Material, further inquiries can be directed to the corresponding author.

AUTHOR CONTRIBUTIONS

TQ: responsible for the main writing of the thesis and the derivation of the formula. SH: responsible for guiding the author's research and revision of the manuscript. JZ: responsible for the provision of experimental data and email communication.

FUNDING

This work was supported by the National Science and Technology Major Project "Zhaotong Shale Gas Exploration and Development Demonstration Project-Comprehensive Mountain Shale Gas Well Productivity Evaluation and Production System Optimization and Application" (Grant No. 2017ZX05063005-019) and The National Natural Science Fund (No. 51574199) administered by the National Natural Science Foundation of China.

REFERENCES

Ambrose, R. J., Hartman, R. C., Diaz-Campos, M., Akkutlu, I. Y., and Sondergeld, C. H. (2012). Shale Gas-In-Place Calculations Part I: New Pore-Scale Considerations. *SPE J.* 17, 219–229. doi:10.2118/131772-PA

Arps, J. J. (1945). Analysis of Decline Curves. *Trans* 160, 228–247. doi:10.2118/945228-G

Boadu, F. K. (2000). Predicting the Transport Properties of Fractured Rocks from Seismic Information: Numerical Experiments. *J. Appl. Geophys.* 44 (2-3), 103–113. doi:10.1016/S0926-9851(99)00020-8

Brunauer, S., Deming, L. S., Deming, W. E., and Teller, E. (1940). On a theory of the van der Waals adsorption of gases. *J. Am. Chem. Soc.* 62, 1723–1732. doi:10.1021/ja01864a025

Brunauer, S., Emmett, P. H., and Teller, E. (1938). Adsorption of Gases in Multimolecular Layers. *J. Am. Chem. Soc.* 60 (2), 309–319. doi:10.1021/ja01269a023

Canel, C. A., and Rosbaco, J. (2006). "Compositional Material Balance: its Application to the Development of an Oil and Gas Field with Retrograde Condensation," in Paper SPE 23647 presented at the Second Latin American Petroleum Engineering Conference, Caracas, Venezuela, January 01, 1992. 117–128 March. doi:10.2118/23647-MS

Chai, D., Yang, G., Fan, Z., and Li, X. (2019). Gas Transport in Shale Matrix Coupling Multilayer Adsorption and Pore Confinement Effect. *Chem. Eng. J.* 370, 1534–1549. doi:10.1016/j.cej.2019.03.276

Chareonsuppanimit, P., Mohammad, S. A., Robinson, R. L., and Gasem, K. A. M. (2012). High-pressure Adsorption of Gases on Shales: Measurements and Modeling. *Int. J. Coal Geology*. 95, 34–46. doi:10.1016/j.coal.2012.02.005

Chen, Y. (1990). The Property of Formation Water Relevant Empirical Equation. *Well Test. Prod. Technology* 11 (3), 31–33.

Clarkson, C. R., and Haghshenas, B. (2013). "Modeling of Supercritical Fluid Adsorption on Organic-Rich Shales and Coal," in Paper SPE 164532 presented at Unconventional Resources Conference-USA held in The Woodlands, Texas, USA, April 2013. doi:10.2118/164532-ms

Curtis, J. B. (2002). Fractured Shale-Gas Systems. *AAPG Bull.* 86 (11), 1921–1938. doi:10.1306/61eeddbe-173e-11d7-8645000102c1865d

Dang, W., Zhang, J., Nie, H., Wang, F., Tang, X., Wu, N., et al. (2020). Isotherms, Thermodynamics and Kinetics of Methane-Shale Adsorption Pair under Supercritical Condition: Implications for Understanding the Nature of Shale Gas Adsorption Process. *Chem. Eng. J.* 383, 123191. doi:10.1016/j.cej.2019.123191

Deng, J., Zhu, W., and Ma, Q. (2014). A New Seepage Model for Shale Gas Reservoir and Productivity Analysis of Fractured Well. *Fuel* 124, 232–240. doi:10.1016/j.fuel.2014.02.001

Fan, L., and Liu, S. (2021). A Novel Experimental System for Accurate Gas Sorption and its Application to Various Shale Rocks. *Chem. Eng. Res. Des.* 165, 180–191. doi:10.1016/j.cherd.2020.10.034

Fianu, J., Gholinezhad, J., and Hassan, M. (2019). Application of Temperature-dependent Adsorption Models in Material Balance Calculations for Unconventional Gas Reservoirs. *Heliyon* 5 (5), e01721. doi:10.1016/j.heliyon.2019.e01721

Fripiat, J. J., Gatineau, L., and Van Damme, H. (1986). Multilayer Physical Adsorption on Fractal Surfaces. *Langmuir* 2 (5), 562–567. doi:10.1021/la00071a006

Gu, N., Zhu, X., and Xing, L. (2014). Oil and Gas Field Development. *Nat. Gas oil* 32 (6), 50–58.

Hu, S., Hu, X., He, L., and Chen, W. (2019). A New Material Balance Equation for Dual-Porosity Media Shale Gas Reservoir. *Energ. Proced.* 158, 5994–6002. doi:10.1016/j.egypro.2019.01.520

Huang, H., Sun, W., Xiong, F., Chen, L., Li, X., Gao, T., et al. (2018). A Novel Method to Estimate Subsurface Shale Gas Capacities. *Fuel* 232, 341–350. doi:10.1016/j.fuel.2018.05.172

Huang, S., Ding, G., Wu, Y., Huang, H., Lan, X., and Zhang, J. (2018). A Semi-analytical Model to Evaluate Productivity of Shale Gas wells with Complex Fracture Networks. *J. Nat. Gas Sci. Eng.* 50, 374–383. doi:10.1016/j.jngse.2017.09.010

Huang, X., and Zhao, Y.-P. (2017). Characterization of Pore Structure, Gas Adsorption, and Spontaneous Imbibition in Shale Gas Reservoirs. *J. Pet. Sci. Eng.* 159 (159), 197–204. doi:10.1016/j.petrol.2017.09.010

Jaroniec, M., Lu, X., Madey, R., and Choma, J. (1989). Extension of the Langmuir Equation for Describing Gas Adsorption on Heterogeneous Microporous Solids. *Langmuir* 5 (3), 839–844. doi:10.1021/la00087a044

Jenkins, C. D., and Boyer, C. M., II (2008). Coalbed- and Shale-Gas Reservoirs. *J. Pet. Technology* 60 (2), 92–99. doi:10.2118/103514-JPT

Langmuir, I. (1918). The Adsorption of Gases on Plane Surfaces of Glass, Mica and Platinum. *J. Am. Chem. Soc.* 40 (9), 1361–1403. doi:10.1063/1.492960910.1021/ja02242a004

Langmuir, I. (2015). The Adsorption of Gases on Plane Surfaces of Glass, Mica and Platinum. *J. Am. Chem. Soc.* 40 (12), 1361–1403.

Li, J., Lu, S., Zhang, P., Cai, J., Li, W., Wang, S., et al. (2020). Estimation of Gas-In-Place Content in Coal and Shale Reservoirs: A Process Analysis Method and its Preliminary Application. *Fuel* 259, 116266. doi:10.1016/j.fuel.2019.116266

Memon, A., Li, A., Jacqueline, N., Kashif, M., and Ma, M. (2020). Study of Gas Sorption, Stress Effects and Analysis of Effective Porosity and Permeability for Shale Gas Reservoirs. *J. Pet. Sci. Eng.* 193, 107370. doi:10.1016/j.petrol.2020.107370

Mengal, S. A., and Wattenbarger, R. A. (2011). "Accounting for Absorbed Gas in Shale Gas Reservoirs," in Paper SPE 141085 presented at SPE Middle East Oil and Gas Show and Conference, Manama, Bahrain, 25–28 September (MS). doi:10.2118/141085

Myers, A. L. (1968). Adsorption of Gas Mixtures-A Thermodynamic Approach. *Ind. Eng. Chem.* 60 (5), 45–49. doi:10.1021/ie50701a007

Myers, A. L., and Prausnitz, J. M. (1965). Thermodynamics of Mixed-Gas Adsorption. *Aiche J.* 11 (1), 121–127. doi:10.1002/aic.690110125

Orozco, Daniel., and Aguilera, Roberto. (2015). "A Material Balance Equation for Stress-Sensitive Shale Gas Reservoirs Considering the Contribution of Free,

Adsorbed and Dissolved Gas," in Paper SPE-175964-MS presented at SPE/CSUR Unconventional Resources Conference held in Calgary, Alberta, Canada, October 2015. 10.2118/175964-MS. doi:10.2118/175964-ms

Pang, Y., Tian, Y., Soliman, M. Y., and Shen, Y. (2019). Experimental Measurement and Analytical Estimation of Methane Absorption in Shale Kerogen. *Fuel* 240, 192–205. doi:10.1016/j.fuel.2018.11.144

Ritter, J. A., and Yang, R. T. (1987). Equilibrium Adsorption of Multicomponent Gas Mixtures at Elevated Pressures. *Ind. Eng. Chem. Res.* 26 (8), 1679–1686. doi:10.1021/ie00068a032

Sang, Y., Chen, H., Yang, S., Guo, X., Zhou, C., Fang, B., et al. (2014). A New Mathematical Model Considering Adsorption and Desorption Process for Productivity Prediction of Volume Fractured Horizontal wells in Shale Gas Reservoirs. *J. Nat. Gas Sci. Eng.* 19, 228–236. doi:10.1016/j.jngse.2014.05.009

Sanyal, D., Ramachandrarao, P., and Gupta, O. P. (2006). A Fractal Description of Transport Phenomena in Dendritic Porous Network. *Chem. Eng. Sci.* 61 (2), 307–315. doi:10.1016/j.ces.2005.06.0010.1016/j.ces.2005.06.005

Shao, X., Pang, X., Li, Q., Wang, P., Chen, D., Shen, W., et al. (2017). Pore Structure and Fractal Characteristics of Organic-Rich Shales: A Case Study of the Lower Silurian Longmaxi Shales in the Sichuan Basin, SW China. *Mar. Pet. Geology.* 80, 192–202. doi:10.1016/j.marpetgeo.2016.11.025

Sun, H., Wang, H., Zhu, S., Nie, H., Liu, Y., Li, Y., et al. (2019). Reserve Evaluation of High Pressure and Ultra-high Pressure Reservoirs with Power Function Material Balance Method. *Nat. Gas Industry B* 6 (5), 509–516. doi:10.1016/j.ngib.2019.03.007

Taghavinejad, A., Sharifi, M., Heidaryan, E., Liu, K., and Ostadhassan, M. (2020). Flow Modeling in Shale Gas Reservoirs: a Comprehensive Review. *J. Nat. Gas Sci. Eng.* 83, 103535. doi:10.1016/j.jngse.2020.103535

Wang, P., Jiang, Z., Ji, W., Zhang, C., Yuan, Y., Chen, L., et al. (2016). Heterogeneity of Intergranular, Intraparticle and Organic Pores in Longmaxi Shale in Sichuan Basin, South China: Evidence from SEM Digital Images and Fractal and Multifractal Geometries. *Mar. Pet. Geology.* 72, 122–138. doi:10.1016/j.marpetgeo.2016.01.020

Wang, Y., Cheng, H., Hu, Q., Liu, L., Jia, L., Gao, S., et al. (2022). Pore Structure Heterogeneity of Wufeng-Longmaxi Shale, Sichuan Basin, China: Evidence from Gas Physisorption and Multifractal Geometries. *J. Pet. Sci. Eng.* 208, 109313. doi:10.1016/j.petrol.2021.109313

Wheaton, R. (2019). Modeling of Gas Flow in Fractured Shale. *Upstream Oil Gas Technology* 1, 100001. doi:10.1016/j.upstre.2020.100001

Wu, K., Chen, Z., and Li, X. (2015). Real Gas Transport through Nanopores of Varying Cross-Section Type and Shape in Shale Gas Reservoirs. *Chem. Eng. J.* 281, 813–825. doi:10.1016/j.cej.2015.07.012

Xiong, F., Rother, G., Gong, Y., and Moortgat, J. (2021). Reexamining Supercritical Gas Adsorption Theories in Nano-Porous Shales under Geological Conditions. *Fuel* 287, 119454. doi:10.1016/j.fuel.2020.119454

Zhang, C.-Y., Chai, X.-S., and Xiao, X.-M. (2015). A Simple Method for Correcting for the Presence of Minor Gases when Determining the Adsorbed Methane Content in Shale. *Fuel* 150, 334–338. doi:10.1016/j.fuel.2015.02.050

Zhang, W., Xu, J., Jiang, R., Cui, Y., Qiao, J., Kang, C., et al. (2017). Employing a Quad-Porosity Numerical Model to Analyze the Productivity of Shale Gas Reservoir. *J. Pet. Sci. Eng.* 157, 1046–1055. doi:10.1016/j.petrol.2017.07.031

Zheng, S., Yao, Y., Liu, D., Cai, Y., Liu, Y., and Li, X. (2019). Nuclear Magnetic Resonance T2 Cutoffs of Coals: A Novel Method by Multifractal Analysis Theory. *Fuel* 241, 715–724. doi:10.1016/j.fuel.2018.12.044

Zhou, S., Zhang, D., Wang, H., and Li, X. (2019). A Modified BET Equation to Investigate Supercritical Methane Adsorption Mechanisms in Shale. *Mar. Pet. Geology.* 105, 284–292. doi:10.1016/j.marpetgeo.2019.04.036

Conflict of Interest: The authors declare that the research was conducted in the absence of any commercial or financial relationships that could be construed as a potential conflict of interest.

Publisher's Note: All claims expressed in this article are solely those of the authors and do not necessarily represent those of their affiliated organizations, or those of the publisher, the editors, and the reviewers. Any product that may be evaluated in this article, or claim that may be made by its manufacturer, is not guaranteed or endorsed by the publisher.